

## NUMERICAL STUDY OF A STOCHASTIC DAMPED WAVE EQUATION

QUANYONG ZHU<sup>1,\*</sup> AND QUANXIANG WANG<sup>2,3</sup>

<sup>1</sup>Department of Mathematics, Lishui University, Lishui 323000, China

<sup>2</sup>College of Engineering, Nanjing Agricultural University, Nanjing 210031, China

<sup>3</sup>Jiangsu Key Laboratory for NSLSCS, Nanjing 210023, China

**ABSTRACT.** Numerical treatment for stochastic nonlinear damped wave equation is studied. A discrete algorithm is proposed by incorporating finite volume element scheme with Monte Carlo Sampling method. The influence of an impurity external term and two kinds of damping effects on the propagation of solitons profile is surveyed. Numerical results demonstrate that the scheme is effective to predict the statistics of the nonlinear wave propagation characteristics.

**Key Words.** Stochastic nonlinear damped wave equation; Finite volume element method; Numerical simulation.

**AMS (MOS) Subject Classification.** 39A10, 65C20.

### 1. INTRODUCTION

In this paper, we consider the numerical simulation of high performance to the following stochastic nonlinear damped wave equation

$$(1.1) \quad \partial_{tt}u(x, t) + \beta u(x, t) - \alpha \partial_{xx}u(x, t) = f(u, x, t) + S(x, t) + \eta \partial_{xx}\xi(x, t),$$

where  $\alpha > 0$ ,  $\eta > 0$  and  $\beta$  are all constants,  $S(x, t)$  is damping term,  $\partial_{xx}\xi(x, t)$  is external stochastic force, and  $(x, t) \in [a, b] \times (0, T]$ . The hydrodynamical damping corresponds to  $S(x, t) = \nu \partial_{txx}u$  and the Stokes damping corresponds to  $S(x, t) = -\rho \partial_t u$ , where  $\nu$  and  $\rho$  are positive constants. Suitable initial and boundary conditions are needed, for example, the Dirichlet boundary condition and periodic boundary conditions. In addition, the stochastic force term  $\xi(x, t)$  is Gaussian white noise with mean zero delta-correlated, i.e.,

$$(1.2) \quad E(\xi(x, t)\xi(x', t')) = \delta(x - x')\delta(t - t'),$$

and

$$(1.3) \quad E(\xi(x, t)) = 0,$$

---

\*Corresponding author. E-mail address: quanyongzhu@126.com.

where  $E(\cdot)$  means average, that it is not correlated with the term  $u(x, t_0)$ , i.e.

$$(1.4) \quad E(u(x, t_0)\xi(x, t)) = 0, \quad t > t_0.$$

The noise term fulfill the fluctuation dissipation theorem.

It is well known that this equation can be identified with others in certain special cases. For example, taking  $\alpha = 1$ ,  $\beta > 0$ ,  $f(u, x, t) = 0$ ,  $S(x, t) = -\rho\partial_t u(x, t)$  and ignore the stochastic force, Equation (1.1) is regarded as telegraph equation which simulates many physical phenomena. For some branches of sciences the telegraph equation is more suitable than general diffusion equation in modeling reaction diffusion dynamics. It can be used to describe the propagation of voltage and current signals in coaxial transmissions lines of negligible leakage conductance and resistance. In porous media which fulfil with Darcy law, the propagation of acoustic waves can be simulated by the telegraph equation. Parallel flows of viscous Maxwell fluids is another typical application, see [1] and references therein. In [2], differential transform method is employed to solve telegraph equation and some exact solutions of the equation are derived. However, a telegraph equation supplement with any initial and boundary conditions, to determine the general form of the exact solution is impossible. Alternatively, the application of an efficient numerical method to solve it approximately is realistic. In the last decades, the development of numerical methods for approximating the solutions of telegraph equation have drawn the attention of many researchers in science and engineering, see, for example [3, 4, 5] and so on.

When  $f(u, x, t)$  is a polynomial function with respect to  $u$ , such as  $f(u, x, t) = (a + \beta)u - \theta u^3$  and absent of damping and stochastic force, Equation (1.1) is refer to nonlinear Klein-Gordon (NKG) equation. When  $\beta = 0$ ,  $S(x, t) = -\rho\partial_t u$ ,  $f(u, x, t) = \gamma(x)\sin(u)$  and without noise effect, Equation (1.1) degenerates into the so called Sine-Gordon (SG) equation or damped Sine-Gordon (DSG) equation. Essentially, the NKG equation is a relativistic version of the Schrödinger equation which is the appropriate model to describe the wave function of the particle that is charge-neutral, spinless with relativistic effects. These equations are of great importance in quantum mechanics and have significant applications in many physical realms. For example, the interaction of Langmuir wave and the ion acoustic wave in a plasma physics, the propagation of fluxion in Josephson junctions between two superconductors, the continuum limit of the Frenkel-Kontorova model related to the dislocations in solids, the electromagnetic wave propagation in semiconductor superlattices, charge density waves and waves in liquid helium, the field theory. In condensed matter physics, it was proposed to describe structural phase transitions and the dynamics of domain walls in ferroelectric and ferromagnetic materials. It was used in connection with the polymer physics and as a model for hydrogen bonded chains and so on [6, 7, 8, 9]. A vast applicability of the soliton equation implies soliton phenomena which are

common in various fields of physics. The soliton solutions of the SG equation, DSG equation and NKG equation have been extensively investigated from theoretical and numerical points of view [10, 11, 12]. We refer to [13, 14, 15, 16] and references therein for a detailed survey of numerical algorithms. Concerning the present situation, it is difficult to solve Equation (1.1) analytically with arbitrary initial and boundary conditions and  $f(u, x, t)$ . Consequently, it is desirable to develop high performance numerical methods for problem (1.1).

On account of nonlinear dynamical system in practice, it is important to investigate the effects due to external stochastic forces, dissipations and damping. To some extent, the effect of the Gaussian noise and Stokes damping and/or hydrodynamical damping on the nonlinear wave problem has significant importance. Under the present investigation, we will employ quadratic finite volume element method (FVEM) [17, 18] for discretization in physical space and Monte Carlo Sampling (MCS) method [19, 20] for discretization in random space. Our goal is to survey the effect of a impurity external term and damping on the propagation of various solitons profile and investigate more general quantities than the expectation. The averaged conserved quantities and the averaged amplitude under stochastic noise and damping will be studied in addition.

The layout of the paper is as follows: In section 2 we show that how we use the finite volume element method to approximate the solution. In section 3 we apply the method on the nonlinear damped wave equation. We then proceed to present the results of numerical experiments for nonlinear stochastic damped wave equation in section 4. Last section is dedicated to a brief conclusion.

## 2. NUMERICAL METHODS

**2.1. NUMERICAL SCHEMES.** In this section, finite volume element schemes will be derived with a special emphasis on applications to solve the considered Equation (1.1). The interval of interest  $[a, b]$  can be decomposed into a grid  $T_h$  with nodes

$$(2.1) \quad a = x_0 < x_1 < x_2 < \dots < x_{N-1} < x_N = b.$$

Denote  $T_h = \{I_i : I_i = [x_{i-1}, x_i], i = 1, 2, \dots, N\}$ . In order to derive basis functions of quadratic element, the midpoints  $x_{i-1/2} = (x_i + x_{i-1})/2$  of the element  $I_i$  will be included as the interpolation points. Then we place a dual grid  $T_h^*$  with nodes

$$(2.2) \quad a = x_0 < x_{1/4} < x_{3/4} < \dots < x_{N-3/4} < x_{N-1/4} < x_N = b,$$

where  $x_{i-k/4} = x_i - \frac{k}{4}h, (k = 1, 3, i = 1, 2, \dots, N)$ . Denote  $I_i^* = [x_{i-1/4}, x_{i+1/4}]$  and  $I_{i-1/2}^* = [x_{i-3/4}, x_{i-1/4}]$ .

Select the trial function space  $U_h$  as the quadratic element space of Lagrange type with respect to  $T_h$ . The basis functions with respect to the node  $x_i$  and the

node  $x_{i-1/2}$  are as follows

$$(2.3) \quad \phi_i(x) = \begin{cases} (2|x-x_i|/h-1)(|x-x_i|/h-1), & x_{i-1} \leq x \leq x_{i+1}, \\ 0, & \text{elsewhere,} \end{cases}$$

$$(2.4) \quad \phi_{i-1/2}(x) = \begin{cases} 4(1-(x-x_{i-1})/h)(x-x_{i-1})/h, & x_{i-1} \leq x \leq x_i, \\ 0, & \text{elsewhere.} \end{cases}$$

Then numerical solution  $u_h$  for Equation (1.1) can be uniquely expressed as  $u_h = \sum_{i=1}^N [u_i \phi_i(x) + u_{i-1/2} \phi_{i-1/2}(x)]$ , where  $u_i = u_h(x_i, t)$ ,  $u_{i-1/2} = u_h(x_{i-1/2}, t)$ . So in the element  $I_i$ , we have

$$(2.5) \quad \begin{aligned} u_h &= u_{i-1}(2\mu-1)(\mu-1) + 4u_{i-1/2}\mu(1-\mu) + u_i(2\mu-1)\mu \\ &= (\mu^2, \mu, 1) \begin{pmatrix} 2 & -4 & 2 \\ -3 & 4 & -1 \\ 1 & 0 & 0 \end{pmatrix} \begin{pmatrix} u_{i-1} \\ u_{i-1/2} \\ u_i \end{pmatrix}, \end{aligned}$$

$$(2.6) \quad \begin{aligned} u'_h &= u_{i-1}(4\mu-3)/h + u_{i-1/2}(-8\mu+4)/h + u_i(4\mu-1)/h \\ &= (\mu, 1) \begin{pmatrix} -4 & 4 \\ 3 & -1 \end{pmatrix} \begin{pmatrix} (u_{i-1/2} - u_{i-1})/h \\ (u_i - u_{i-1/2})/h \end{pmatrix}, \end{aligned}$$

where  $\mu = (x - x_{i-1})/h$ .

The test function space  $V_h$  corresponding to  $T_h^*$  is taken as the piecewise constant function space. The test basis functions of the nodes  $x_j$  and  $x_{j-1/2}$  are

$$(2.7) \quad \psi_j(x) = \begin{cases} 1, & x_{j-1/4} \leq x \leq x_{j+1/4}, \\ 0, & \text{elsewhere,} \end{cases}$$

$$(2.8) \quad \psi_{j-1/2}(x) = \begin{cases} 1, & x_{j-3/4} \leq x \leq x_{j-1/4}, \\ 0, & \text{elsewhere.} \end{cases}$$

By introducing an intermediate variable  $v(x, t) = \partial_t u(x, t)$ , Equation (1.1) can be transformed to an equivalent form of two differential equations of first-order in time

$$(2.9) \quad \begin{cases} \partial_t u(x, t) = v(x, t), \\ \partial_t v(x, t) + \beta u(x, t) - \alpha u_{xx}(x, t) = f(u, x, t) + S(x, t) + \eta \partial_{xx} \xi(x, t). \end{cases}$$

Use any function  $\psi_j, \psi_{j-1/2} \in V_h$  to multiply both sides of the second equation of Equation (2.9) and integrate by parts on the region  $[a, b]$ , we can obtain the semi-discrete schemes as following

$$(2.10) \quad \begin{cases} a((v_h)_t, \psi_j) + b(\beta u_h, \psi_j) - c((\alpha u_h)_{xx}, \psi_j) = (f, \psi_j) + (S, \psi_j) + (\eta \partial_{xx} \xi, \psi_j), \\ a((v_h)_t, \psi_{j-1/2}) + b(\beta u_h, \psi_{j-1/2}) - c((\alpha u_h)_{xx}, \psi_{j-1/2}) \\ \quad = (f, \psi_{j-1/2}) + (S, \psi_{j-1/2}) + (\eta \partial_{xx} \xi, \psi_{j-1/2}), \end{cases}$$

where  $(\cdot, \cdot)$  represents the inner product of  $L^2([a, b])$ ,  $j = 1, 2, \dots, N$ ,

$$a((v_h)_t, \psi_j) = \int_a^b \dot{v} \psi_j dx = \int_{x_{j-1/4}}^{x_{j+1/4}} \dot{v} dx = \frac{h}{2} \dot{v}_j,$$

$$a((v_h)_t, \psi_{j-1/2}) = \int_a^b \dot{v} \psi_{j-1/2} dx = \int_{x_{j-3/4}}^{x_{j-1/4}} \dot{v} dx = \frac{h}{2} \dot{v}_{j-1/2},$$

$$b(\beta u_h, \psi_j) = \int_a^b \beta u_h \psi_j dx = \int_{x_{j-1/4}}^{x_{j+1/4}} \beta u_h dx = \frac{h}{2} \beta u_j,$$

$$b(\beta u_h, \psi_{j-1/2}) = \int_a^b \beta u_h \psi_{j-1/2} dx = \int_{x_{j-3/4}}^{x_{j-1/4}} \beta u_h dx = \frac{h}{2} \beta u_{j-1/2},$$

$$c((\alpha u_h)_{xx}, \psi_j) = - \int_a^b \alpha u_x \psi_j' dx = \alpha u_h'(x_{j+1/4}) - \alpha u_h'(x_{j-1/4}) = \frac{2}{h} \alpha (u_{j-1/2} - 2u_j + u_{j+1/2}),$$

$$c((\alpha u_h)_{xx}, \psi_{j-1/2}) = - \int_a^b \alpha u_x \psi_{j-1/2}' dx = \alpha u_h'(x_{j-1/4}) - \alpha u_h'(x_{j-3/4}) = \frac{2}{h} \alpha (u_{j-1} - 2u_{j-1/2} + u_j),$$

$$(f, \psi_j) = \int_a^b f \psi_j dx = \int_{x_{j-1/4}}^{x_{j+1/4}} f dx = \frac{h}{2} f_j,$$

$$(f, \psi_{j-1/2}) = \int_a^b f \psi_{j-1/2} dx = \int_{x_{j-3/4}}^{x_{j-1/4}} f dx = \frac{h}{2} f_{j-1/2},$$

$$(2.11) \quad \tilde{S}_j = (S, \psi_j) = \begin{cases} \frac{2}{h} \nu (v_{j-1/2} - 2v_j + v_{j+1/2}), & \text{hydrodynamical damping} \\ -\frac{h}{2} \nu v_j, & \text{Stokes damping} \end{cases}$$

$$(2.12) \quad \tilde{S}_{j-1/2} = (S, \psi_{j-1/2}) = \begin{cases} \frac{2}{h} \nu (v_{j-1} - 2v_{j-1/2} + v_j), & \text{hydrodynamical damping} \\ -\frac{h}{2} \nu v_{j-1/2}, & \text{Stokes damping} \end{cases}$$

$$(\eta \partial_{xx} \xi, \psi_j) = \frac{2\eta}{h} (\xi_{j-1/2} - 2\xi_j + \xi_{j+1/2}),$$

$$(\eta \partial_{xx} \xi, \psi_{j-1/2}) = \frac{2\eta}{h} (\xi_{j-1} - 2\xi_{j-1/2} + \xi_j),$$

where  $\cdot = \frac{d}{dt}$ ,  $j = 1, 2, \dots, N$ . Then we can obtain the semi-discrete finite volume element schemes as follows

$$(2.13) \quad \begin{cases} \dot{u}_j = v_j, \\ \frac{h^2}{4} \dot{v}_j + \frac{h^2}{4} \beta u_j - \alpha(u_{j-1/2} - 2u_j + u_{j+1/2}) \\ \quad = \frac{h^2}{4} f_j + \tilde{S}_j + \eta(\xi_{j-1/2} - 2\xi_j + \xi_{j+1/2}), \\ \dot{u}_{j-1/2} = v_{j-1/2}, \\ \frac{h^2}{4} \dot{v}_{j-1/2} + \frac{h^2}{4} \beta u_{j-1/2} - \alpha(u_{j-1} - 2u_{j-1/2} + u_j) \\ \quad = \frac{h^2}{4} f_{j-1/2} + \tilde{S}_{j-1/2} + \eta(\xi_{j-1} - 2\xi_{j-1/2} + \xi_j), \end{cases}$$

where  $\tilde{S}_j, \tilde{S}_{j-1/2}$  given by (2.11) and (2.12),  $\xi_{j-1}$  and  $\xi_{j-1/2}$  denotes Gaussian white noise at nodes  $x_j$  and  $x_{j-1/2}$ , respectively.

For the purpose of preserving global second-order accuracy of full-discrete finite volume element scheme and to cut down the computational consumption, time derivative will be discretized in the Crank-Nicolson type. For the first two equations in Equation (2.13), the schemes are

$$(2.14) \quad \begin{cases} \frac{u_j^{n+1} - u_j^n}{\Delta t} = \frac{1}{2} v_j^{n+1} + \frac{1}{2} v_j^n, \\ \frac{v_j^{n+1} - v_j^n}{\Delta t} = \frac{1}{2} [-\beta u_j^{n+1} + \frac{4}{h^2} (u_{j-1/2}^{n+1} - 2u_j^{n+1} + u_{j+1/2}^{n+1}) + f_j^{n+1} \\ \quad + \frac{2}{h} \tilde{S}_j + \frac{4\eta}{h^2} (\xi_{j-1/2}^{n+1} - 2\xi_j^{n+1} + \xi_{j+1/2}^{n+1})] \\ \quad + \frac{1}{2} [-\beta u_j^n + \frac{4}{h^2} (u_{j-1/2}^n - 2u_j^n + u_{j+1/2}^n) + f_j^n \\ \quad + \frac{2}{h} \tilde{S}_j + \frac{4\eta}{h^2} (\xi_{j-1/2}^n - 2\xi_j^n + \xi_{j+1/2}^n)], \end{cases}$$

where  $\Delta t, h$  time step size and space step size, respectively.

**2.2. VALIDATION OF NUMERICAL SCHEMES.** For the sake of avoiding the numerical chaos and its interference with the stochastic perturbations, it is important to check whether the scheme reproduce as much as possible the dynamics of the underlying continuous system in absence of stochastic perturbations with individual initial and boundary conditions. Although our aim is not to investigate the deterministic nonlinear wave equation. We want to be sure that the situation observed in the next sections are owing to the stochastic effect and/or damping but not numerical errors. A least square fit result of convergence order and residual will be computed at each experiment which are denoted by  $r$  and  $Resid.$   $\log(error) = \log C + r \log \Delta t$ . A least square fit for  $\log C$  and  $r$  will be computed at each experiment

### A. General initial boundary value problems

To begin with, we set  $\alpha = 1, \beta = -1$  in Equation (1.1) without damping and noise, choosing a right initial data is a rather subtle issue, we using  $u(x, 0) = \sin(\pi x)$  in this case.  $f(x, t) = (\pi^2 - 0.75)e^{-0.5t} \sin(\pi x)$ ,  $(x, t) \in [0, 1] \times [0, 1]$  and Dirichlet boundary condition will be employed. Its exact solution is  $u(x, t) = e^{-0.5t} \sin(\pi x)$ .

TABLE 1. Numerical results of  $u$  with  $h = 2\Delta t$ , case A.

$N$	$M$	$L_2$ error	$r$	$L_\infty$ error	$r$
8	16	$3.9409 \times 10^{-4}$		$5.7000 \times 10^{-3}$	
16	32	$9.8522 \times 10^{-5}$	4.0012(2.0013)	$1.4000 \times 10^{-3}$	4.0714(2.0255)
32	64	$2.4147 \times 10^{-5}$	4.0801(2.0286)	$3.5361 \times 10^{-4}$	3.9592(1.9852)
64	128	$5.9320 \times 10^{-6}$	4.0706(2.0253)	$8.8396 \times 10^{-5}$	4.0003(2.0001)
128	256	$1.4120 \times 10^{-6}$	4.2011(2.0708)	$2.2099 \times 10^{-5}$	4.0000(2.0000)
256	512	$3.4421 \times 10^{-7}$	4.1021(2.0364)	$5.5247 \times 10^{-6}$	4.0003(2.0001)
LSF		$Resid = 0.0300$	$r = 2.0344$	$Resid = 0.0126$	$r = 2.0003$

The error in  $L_2$  and  $L_\infty$  norms for this case and solutions with the above parameters have been computed at  $t = 1$ . They are displayed in Tables 1 for  $h = 2\Delta t$ , where  $\Delta t$  is time step size,  $M$  the number of temporal integer node. In the parentheses, we list the results of the corresponding convergence order defined as  $\log(ratio)/\log(2)$ . Figure 1 is drawn according to the data in Table 1. Examination of the Table 1 and Figure 1, we obtain some conclusions as follows. (1) It is shown that the error measures of the finite volume element scheme diminish approximately quadratically as the space step size and time step size are simultaneously halved, which is consistent with the use of quadratic element space of Lagrange type. (2) The proposed scheme is robust with respect to time step size. In the following numerical simulation, we will take  $h = 2\Delta t$ . (3) We can see from Figure 1 that the dashed line and the asterisks line are almost parallel to the diamond line, which indicate that the numerical solutions of  $u$  obtained by our scheme have second-order accuracy both in the discrete  $L_\infty$  and  $L_2$  norms. (4) Least square fit results demonstrate the second order convergency as well. (5) The scheme have a large zone of stability.

**B. Soliton solutions cases**

As another example, we consider the situation when  $\alpha = \beta^2$ ,  $\beta > 0$ ,  $S(x, t) = 0$ ,  $\eta = 0$  and  $f(u, x, t) = \gamma u^3$  in Equation (1.1). In such a case, the problem turn's out to be a kind of the NKG equations. Supplemented with Dirichlet boundary condition and initial condition

$$(2.15) \quad u(x, 0) = \sqrt{\frac{2\beta}{\gamma}} \operatorname{sech}(\kappa x),$$

it is well known that the equation bear's the so called soliton solution as follows,

$$(2.16) \quad u(x, t) = \sqrt{\frac{2\beta}{\gamma}} \operatorname{sech}(\kappa(x - ct)),$$

where  $\kappa = \sqrt{\frac{\beta}{\beta^2 - c^2}}$ ,  $c$  positive constant represents velocity. This problem with different parameters  $\beta, \gamma$  and  $c$  is solved by our FVE method with different mesh sizes with

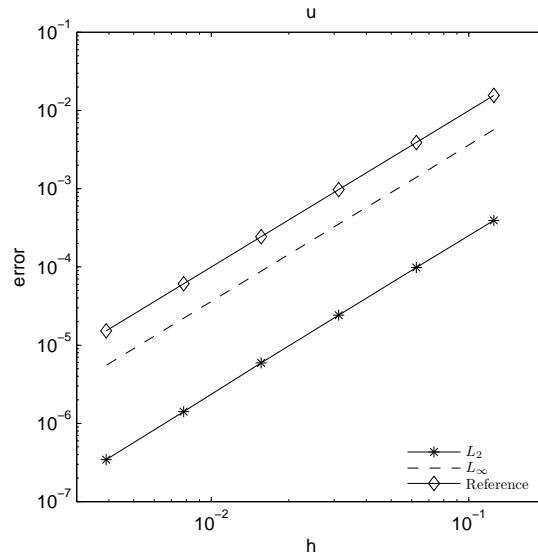


FIGURE 1. Convergence order plot of the numerical solution of  $u$  for case A with  $h = 2\Delta t$ .

TABLE 2. Numerical results of  $u$  in case B with different parameters with  $h = 2\Delta t$ .

$h$	$L_2$ error	$r$	$L_\infty$ error	$r$
$\beta = 1, \gamma = 2, c = 0.8$				
1/2	$2.2000 \times 10^{-2}$		$6.5300 \times 10^{-2}$	
1/4	$5.1000 \times 10^{-3}$	4.3137(2.1089)	$1.7200 \times 10^{-2}$	3.7965(1.9247)
1/8	$1.2000 \times 10^{-3}$	4.2500(2.0875)	$4.2000 \times 10^{-3}$	4.0952(2.0339)
1/16	$2.9697 \times 10^{-4}$	4.0408(2.0146)	$1.0000 \times 10^{-3}$	4.2000(2.0704)
LSF	$Resid = 0.0336$	$r = 2.0721$	$Resid = 0.0517$	$r = 2.0121$
$\beta = 1, \gamma = 10, c = 0.85$				
1/2	$1.5500 \times 10^{-2}$		$4.0100 \times 10^{-2}$	
1/4	$3.6005 \times 10^{-3}$	4.3056(2.1062)	$1.3500 \times 10^{-2}$	2.9704(1.5706)
1/8	$8.5948 \times 10^{-4}$	4.1886(2.0665)	$3.2001 \times 10^{-3}$	4.2188(2.0768)
1/16	$2.0963 \times 10^{-4}$	4.1000(2.0356)	$7.7751 \times 10^{-4}$	4.1157(2.0411)
LSF	$Resid = 0.0245$	$r = 2.0691$	$Resid = 0.1834$	$r = 1.9143$

$x \in [-5, 9]$ . The computational results including discrete  $L_\infty, L_2$ -errors are given in Table 2. These numerical results are also plotted in Figure 2.

As what we have anticipated, it is shown from Table 2 that the accuracy of  $L_\infty$  and  $L_2$  norm errors of  $u$  are increasing with  $h$  decreasing under different parameters. It is also shown that approximation order of  $u$  in different norms is almost two order, respectively. Figure 2 shows the discrete scheme has a 2 order convergency in  $L_\infty$  and  $L_2$  norms. In right column we see that the dashed line's slope is slightly less

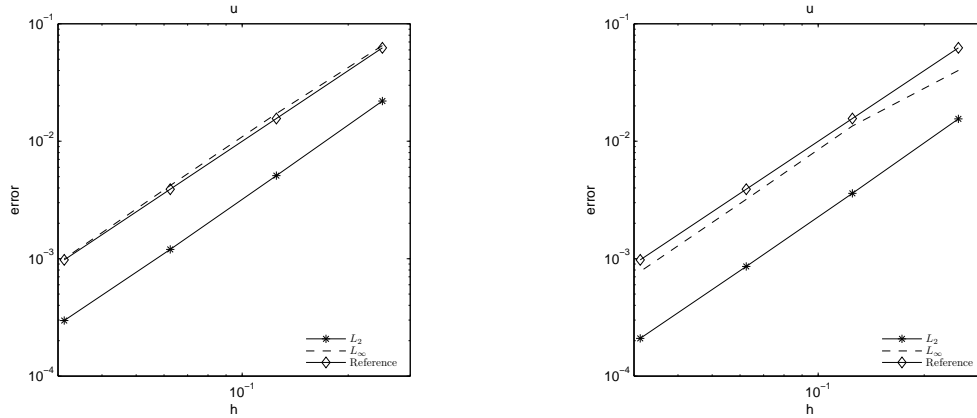


FIGURE 2. Convergence order plots of the numerical solutions of  $u$  for case B with different parameter with  $h = 2\Delta t$ ,  $\beta = 1$ ,  $\gamma = 2$ ,  $c = 0.8$  in left and  $\beta = 1$ ,  $\gamma = 10$ ,  $c = 0.85$  in right.

than 2 at beginning which owing to the step size is coarse at the start. This is the experiment with analytic solutions against which we can compare the numerical solution to illustrate the efficiency and accuracy order of the scheme in both the temporal and spatial dimensions. Examination of the numerical results in Table 2 and Figure 2, it is obvious that if computational accuracy of  $10^{-4}$  is enough to satisfy practical engineer requirement, we can not only adopt larger temporal step, but also use cheaper CPU cost to obtain satisfactory computational results. This further implies that the proposed algorithm is a potential candidate to be adopted in large scale scientific computing.

As we know, an important property of this kind of problem is the conservation of energy, linear momentum and angular momentum except for a well know conserved quantity for the equation,  $MA = \int u dx$ . Without loss of generality, we rewrite the equation in the form of

$$(2.17) \quad \partial_{tt}u - \partial_{xx}u + F(u) = 0,$$

where  $\int_0^u F(u)du = G(u)$ , see for example  $F(u) = k_1u + k_2u^3$  for classical NKG equation and  $F(u) = \sin u$  for SG equation.

**Lemma 2.1.** *Nonlinear equation (2.17) preserves three conserved quantities, they are the energy*

$$E(t) = \int_{-\infty}^{\infty} \left[ \frac{1}{2}(\partial_t u(x, t))^2 + \frac{1}{2}|\partial_x u(x, t)|^2 + G(u(x, t)) \right] dx = E(0), \quad t \in T,$$

*the linear momentum*

$$LM(t) = \int_{-\infty}^{\infty} \partial_t u(x, t)\partial_x u(x, t)dx = LM(0), \quad t \in T,$$

and the angular momentum

$$AM(t) = \int_{-\infty}^{\infty} \left[ x \left( \frac{1}{2} (\partial_t u(x, t))^2 + \frac{1}{2} |\partial_x u(x, t)|^2 + G(u(x, t)) \partial_t u(x, t) \right) + t \partial_t u(x, t) \partial_x u(x, t) \right] dx = AM(0), \quad t \in T.$$

**Proof 1.** We proceed to prove this lemma. Firstly, we can multiply Equation (2.17) by  $\partial_t u(x, t)$  and integrate over  $[-\infty, \infty]$ , by doing so we have

$$(2.18) \quad \int_{-\infty}^{\infty} \partial_t \left[ \frac{1}{2} (\partial_t u(x, t))^2 + \frac{1}{2} |\partial_x u(x, t)|^2 + G(u(x, t)) \right] dx - \int_{-\infty}^{\infty} \partial_x (\partial_x u(x, t) \partial_t u(x, t)) dx = 0.$$

From Equation (2.18) we get the conservation of energy

$$(2.19) \quad \partial_t E(t) = \int_{-\infty}^{\infty} \partial_t \left[ \frac{1}{2} (\partial_t u(x, t))^2 + \frac{1}{2} |\partial_x u(x, t)|^2 + G(u(x, t)) \right] dx = 0.$$

A similar heuristic argument, by multiplying  $\partial_x u(x, t)$  on Equation (2.17) and integrating over  $[-\infty, \infty]$ , we have

$$(2.20) \quad \int_{-\infty}^{\infty} \partial_t (\partial_x u(x, t) \partial_t u(x, t)) dx - \int_{-\infty}^{\infty} \partial_x \left[ \frac{1}{2} (\partial_t u(x, t))^2 + \frac{1}{2} |\partial_x u(x, t)|^2 - G(u(x, t)) \right] dx = 0.$$

It can easily be checked from Equation (2.20) that the linear momentum is conserved

$$(2.21) \quad \partial_t LM(t) = \int_{-\infty}^{\infty} \partial_t (\partial_x u(x, t) \partial_t u(x, t)) dx = 0.$$

The next thing to do in the proof is multiplying  $x \partial_t u(x, t)$  on Equation (2.17), it is easy to see that

$$(2.22) \quad x \partial_t u(x, t) (\partial_{tt} u(x, t) - \partial_{xx} u(x, t) + G(u(x, t))) = 0,$$

similarly, multiplying  $t \partial_x u(x, t)$  on Equation (2.17), we have

$$(2.23) \quad t \partial_x u(x, t) (\partial_{tt} u(x, t) - \partial_{xx} u(x, t) + G(u(x, t))) = 0,$$

subtracting (2.22) by (2.23) and integrating over  $[-\infty, \infty]$ , we have

$$(2.24) \quad \int_{-\infty}^{\infty} \partial_t \left[ x \left( \frac{1}{2} (\partial_t u(x, t))^2 + \frac{1}{2} |\partial_x u(x, t)|^2 + G(u(x, t)) \partial_t u(x, t) \right) + t \partial_t u(x, t) \partial_x u(x, t) \right] dx - \int_{-\infty}^{\infty} \partial_x \left[ (x \partial_x u(x, t)) \partial_t u(x, t) + t \left( \frac{1}{2} (\partial_t u(x, t))^2 + \frac{1}{2} |\partial_x u(x, t)|^2 - G(u(x, t)) \right) \right] dx = 0.$$

From (2.24) we can obtain the conservation of angular momentum

$$(2.25) \quad \partial_t AM(t) = \int_{-\infty}^{\infty} \partial_t \left[ x \left( \frac{1}{2} (\partial_t u(x, t))^2 + \frac{1}{2} |\partial_x u(x, t)|^2 + G(u(x, t)) \partial_t u(x, t) \right) + t \partial_t u(x, t) \partial_x u(x, t) \right] dx = 0.$$

This completes the proof of Lemma 2.1.

It is interesting to see whether these quantities remain invariant when there are stochastic force and/or damping effects. So we consider the following relative error

$$(2.26) \quad I_1(t) = (MA(t) - MA(0))/MA(0),$$

$$(2.27) \quad I_2(t) = (E(t) - E(0))/E(0),$$

$$(2.28) \quad I_3(t) = (LM(t) - LM(0))/LM(0).$$

We perform a simulation at resolution with  $2\Delta t = h$  for case B under different parameters, where  $(x, t) \in [-5, 9] \times (0, 6]$ . The evolution of  $I_1, I_2$  and  $I_3$  are displayed in Figure 3. The amplitude of variation of the quantities  $I_1, I_2$  and  $I_3$  are all very small in our simulation, which is only about  $10^{-5}$ . We can see that our discrete scheme may possess intrinsic invariants are very close to the given initial condition. Noticing that the error are small, which indicates that the schemes are efficient and robust for the considered problem.

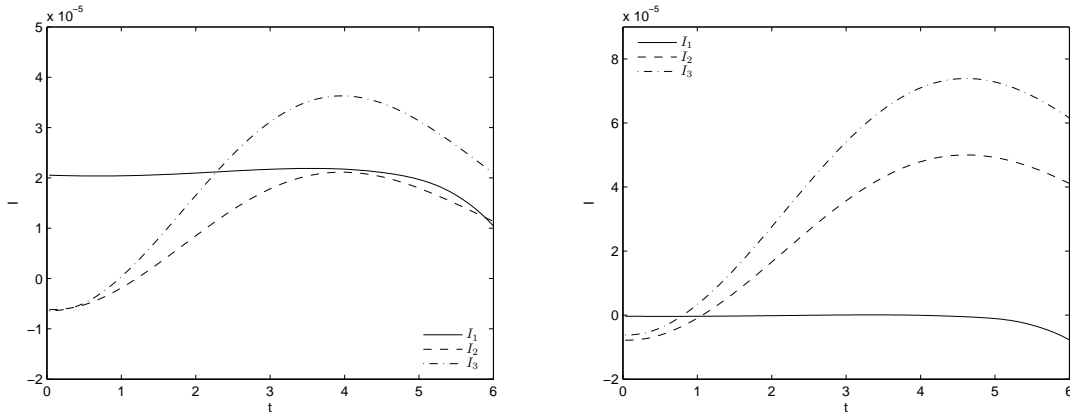


FIGURE 3. Variation of  $I_1, I_2, I_3$ , left:  $\beta = 1, \gamma = 2, c = 0.8$ , right:  $\beta = 1, \gamma = 10, c = 0.85$ , case B.

### 3. DAMPED WAVE EQUATION

**3.1. THE STOKES DAMPING.** In this section, we study the influence of damping on the propagation of solitary wave. Two kinds of damping, namely Stokes damping and hydrodynamical damping on different soliton will be investigated. The three important quantities  $I_1, I_2$  and  $I_3$  will be measured under each circumstance.

(1) To begin with, we consider the situation of  $\alpha = \beta^2, \beta > 0, S(x, t) = -\rho \partial_t u, \eta = 0$  and  $f(u, x, t) = \gamma u^3$  in Equation (1.1). The initial, boundary conditions and parameters are chosen the same as in the previous section. Figure 4 reports the propagation of soliton with  $\beta = 1, \gamma = 2, c = 0.8$  under Stokes damping with

different strength (left for strong damping where  $\rho = 5$  and right for weak damping where  $\rho = 0.5$ ). We can see that the profile is changed by Stokes damping in both circumstances. More precisely, the decay magnitude under strong damping is bigger than the weak damping case. Actually, the profile is destroyed severely under the strong Stokes damping. Figure 5 shows the variation of  $I_1$ ,  $I_2$  and  $I_3$ . As can be seen

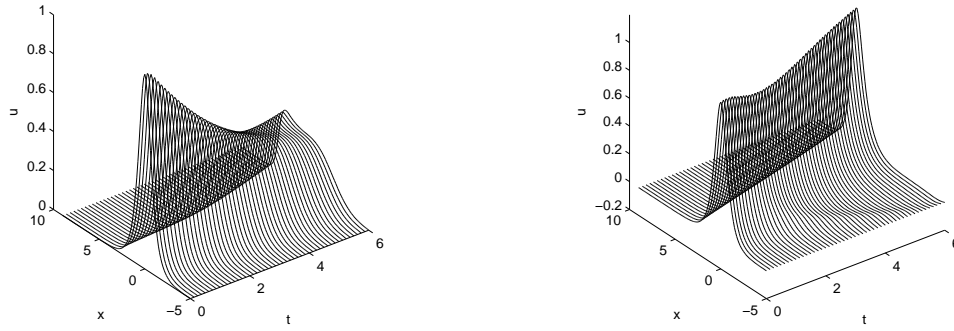


FIGURE 4. Propagation of soliton with Stokes damping, where  $\beta = 1$ ,  $\gamma = 2$ ,  $c = 0.8$ . Left:  $\rho = 5$ , right:  $\rho = 0.5$ .

from Figure 5 (left),  $I_1$  almost keeps invariant when compared to  $I_2$  and  $I_3$ . It seems that the  $I_2$  decrease with time linearly. While  $I_3$  decrease quickly at the first one half time, then it decrease very slowly after a minor rebound. Roughly speaking,  $I_2$  and  $I_3$  decrease with time under the Stokes damping with strong strength. From Figure 5 (right), we can see that  $I_1$  keeps almost invariant when compared to  $I_2$  and  $I_3$ , which is similar to the left case. Concerning the quantities  $I_2$  and  $I_3$ , first decrease then increase with time are observed. Within the undergoing simulation, we can find out that the quantities  $I_2$  and  $I_3$  at the beginning are almost equal to the values at the end moment. These numerical results indicate that the Stokes damping will destroy the soliton profile to some extent while the quantities  $I_1$ ,  $I_2$  and  $I_3$  will behavior distinctly under the two situation. To some extent,  $I_1$  is invariant which indicates that the  $MA$  is conserved.

(2) We now step to the situation of kink wave solution. Under this situation we have  $\alpha = \beta^2$ ,  $\beta > 0$ ,  $S(x, t) = -\rho \partial_t u$ ,  $\eta = 0$  and  $f(u, x, t) = \gamma u^3$  in Equation (1.1). The initial condition takes the form as follows

$$(3.1) \quad u(x, 0) = \sqrt{\frac{\beta}{\gamma}} \tanh h(\kappa x),$$

where  $\kappa = \sqrt{\frac{\beta}{2(c^2 - \beta^2)}}$ ,  $c$  positive constant. We take  $\rho = 5$  and  $\rho = 0.5$  for Stokes damping and simulate the kink wave in  $(x, t) \in [-5, 9] \times (0, 5]$ , where  $\beta = 1$ ,  $\gamma = 2$ ,  $c = 1.1$ . In Figure 6 the propagation of kink wave when  $\rho = 0.5$  is displayed. The

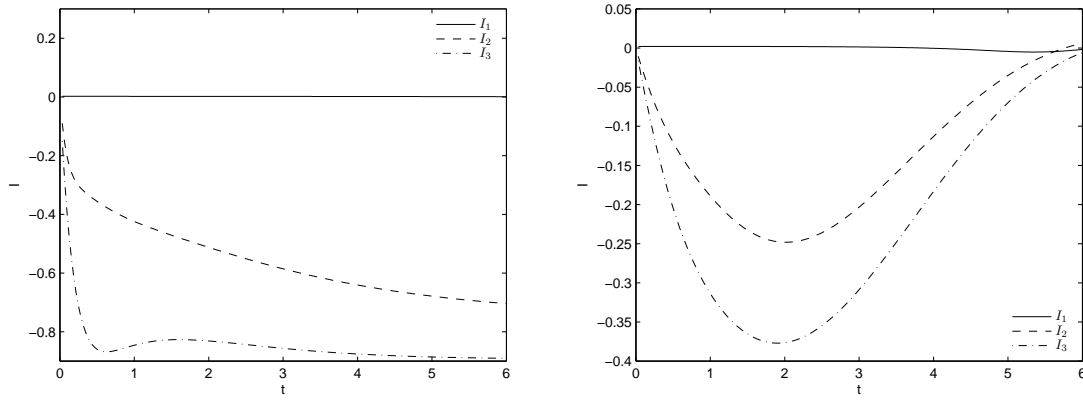


FIGURE 5. Variation of  $I_1, I_2, I_3$  with Stokes damping, where  $\beta = 1$ ,  $\gamma = 2$ ,  $c = 0.8$ . Left:  $\rho = 5$ , right:  $\rho = 0.5$ .

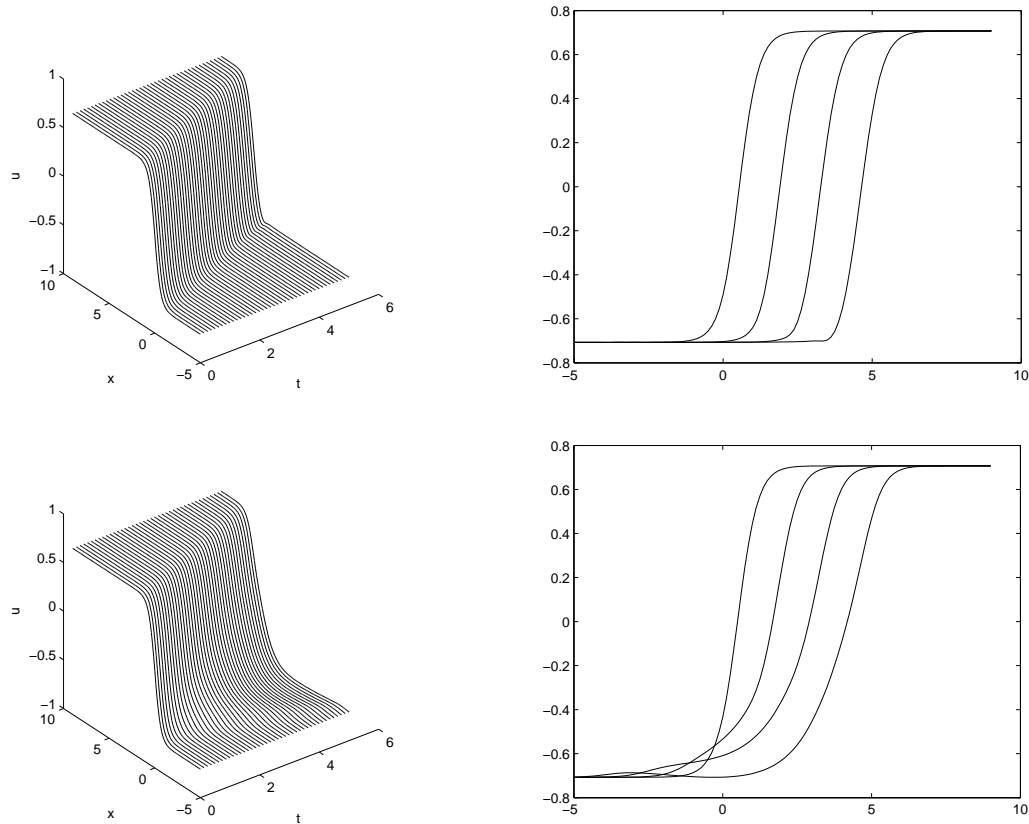


FIGURE 6. Top left: Propagation of kink without damping, top right: snapshot of kink profile without damping. Bottom left: Propagation of kink with Stokes damping, bottom right: snapshot of kink profile with Stokes damping, where  $\rho = 0.5$ ,  $\beta = 1$ ,  $\gamma = 2$ ,  $c = 1.1$ .

destruction of the kink profile is observed. The variation of  $I_2$  and  $I_3$  are given in Figure 7 for  $\rho = 5$  and  $\rho = 0.5$ . From the left plot of Figure 7 we can see that the fluctuation of  $I_2$  is smaller than the  $I_3$ .  $I_2$  is decrease with time and finally

located around zero which indicate the quantity  $E$  is almost conserved except for the beginning time interval. On the other hand,  $I_3$  is decreased rapidly at the first short time frame and then keeps a roughly steady state at the rest temporal interval. The variation of  $I_2$  in the right plot of Figure 7 is similar to the left case, however, the fluctuation in right is smaller than the left plot. It can be deduced from the two plots of  $I_2$  that the quantity  $E$  under small Stokes damping is more steady than the strong damping case. Concerning  $I_3$  in the right plot of Figure 7, it is decrease from 0 to  $-0.48$  on the first half temporal interval, then keeps a relatively steady state on the second half time interval. Once again, these numerical results demonstrate that the Stokes damping will destroy the kink wave profile, and the quantities  $I_2$  and  $I_3$  will behavior a variation with different amplitude.

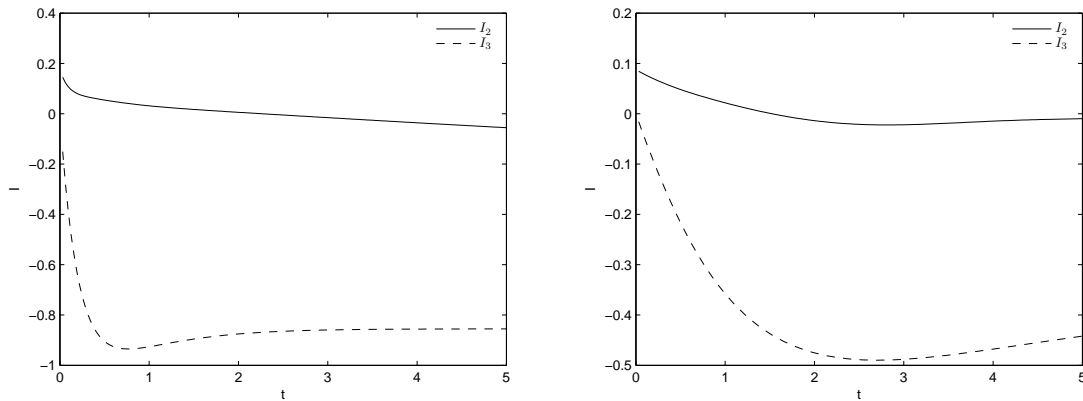


FIGURE 7. Variation of  $I_2, I_3$  with Stokes damping, where  $\beta = 1, \gamma = 2, c = 1.1$ . Left:  $\rho = 5$ , right:  $\rho = 0.5$ .

**3.2. THE HYDRODYNAMICAL DAMPING.** (1) We now consider the evolution of soliton in the presence of hydrodynamical damping. Under this circumstance, we take  $\alpha = \beta^2, \beta > 0, S(x, t) = \nu \partial_{txx} u, \eta = 0$  and  $f(u, x, t) = \gamma u^3$  in Equation (1.1). Initial condition (2.15) and Dirichlet boundary condition will be used and the simulation is took on  $(x, t) \in [-5, 9] \times (0, 6]$ . Figure 8 illustrates the propagation of soliton with  $\nu = 0.1$  and  $\nu = 0.01$  by means of contour plots. Graphically, we can find that the profile is changed by hydrodynamical damping. Nevertheless, the soliton is not totally destroyed. Furthermore, the soliton keep evolve with the speed approximately equal to the initial one which indicated by the slope of the contour curves. The variation of  $I_1, I_2$  and  $I_3$  are shown in Figure 9. In Figure 9,  $I_1$  is almost keep invariant on both plots which indicate that the quantity  $MA$  roughly conserved in the presence of hydrodynamical damping in our simulation. Concerning  $I_2$  and  $I_3$ , they experience a first decrease then increase process in both plots of Figure 9. However, the fluctuations are different. More precisely, the fluctuation on left plot is more broaden than the right plot, which indicate that the oscillation of quantities  $I_2$

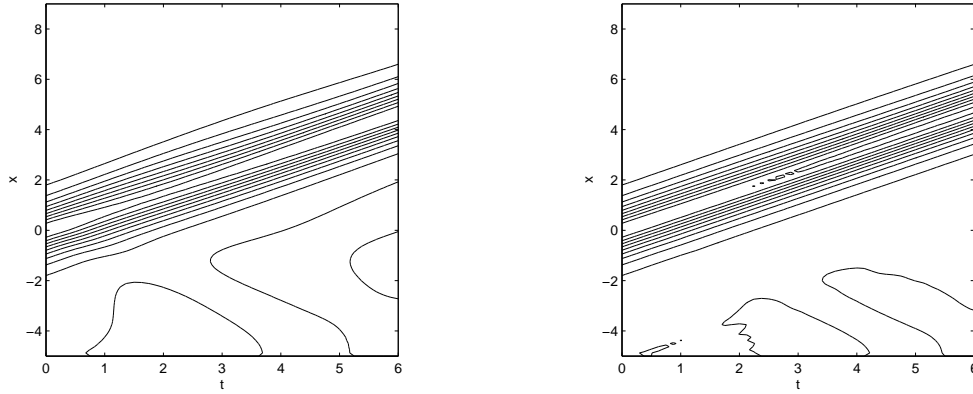


FIGURE 8. Contour plots of soliton with hydrodynamical damping where  $\beta = 1, \gamma = 2, c = 0.8$ . Left:  $\nu = 0.1$ , right:  $\nu = 0.01$ .

and  $I_3$  under strong hydrodynamical damping is more severe than the weak damping. Furthermore,  $I_2$  and  $I_3$  are no longer invariant under both cases in the rigorous meaning. The same experiment has been done with  $\beta = 1, \gamma = 10, c = 0.85$ . Again, we have observed the similar phenomena.

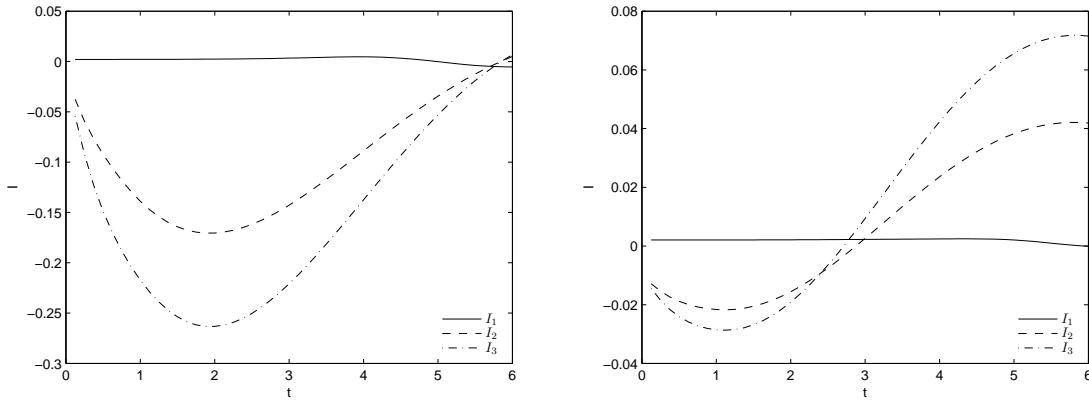


FIGURE 9. Variation of  $I_1, I_2, I_3$  with hydrodynamical damping, where  $\beta = 1, \gamma = 2, c = 0.8$ . Left:  $\nu = 0.1$ , right:  $\nu = 0.01$ .

(2) We take  $\nu = 0.1$  and  $\nu = 0.01$  for hydrodynamical damping and simulate the kink wave in  $(x, t) \in [-5, 9] \times (0, 5]$ , where  $\beta = 1, \gamma = 2, c = 1.1$ . Figure 10 (left) reports the propagation of kink wave when  $\nu = 0.01$ . Figure 10 (right) is the snapshot plot according to the left plot. From the figure we can see that the kink wave is slightly contaminated by the hydrodynamical damping. However, the profile is not destroyed severely. The variation of  $I_2$  and  $I_3$  are presented in Figure 11 (left for  $\nu = 0.1$  and right for  $\nu = 0.01$ ). We see that the fluctuation of the two quantities are relatively small. Roughly speaking, the two quantities are declined linearly with respect to time. However, the amplitudes of the two quantities are distinct. In retrospect the Stokes damping situation, we can conclude that the energy, linear momentum are

no longer keep invariant rigorously. As has been observed, hydrodynamical damping may violate the kink wave shape to some extent and shift the values of  $E$ ,  $LM$  in our study.

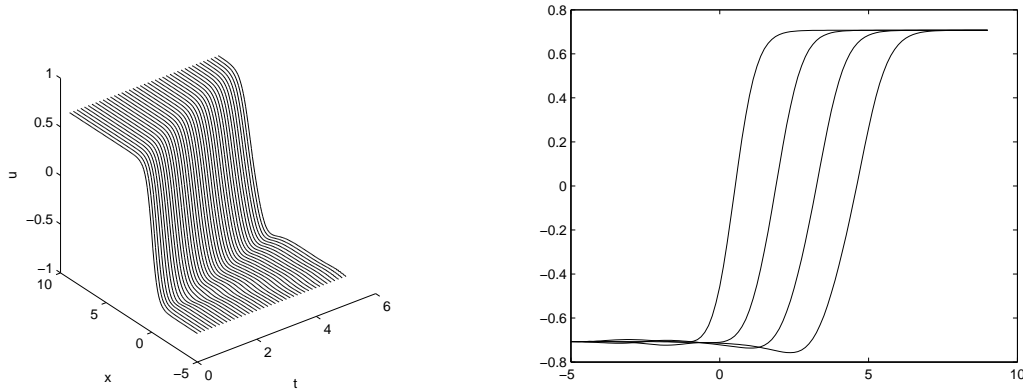


FIGURE 10. Left: propagation of kink with hydrodynamical damping, right: snapshot of kink profile with hydrodynamical damping, where  $\nu = 0.01$ ,  $\beta = 1$ ,  $\gamma = 2$ ,  $c = 1.1$ .

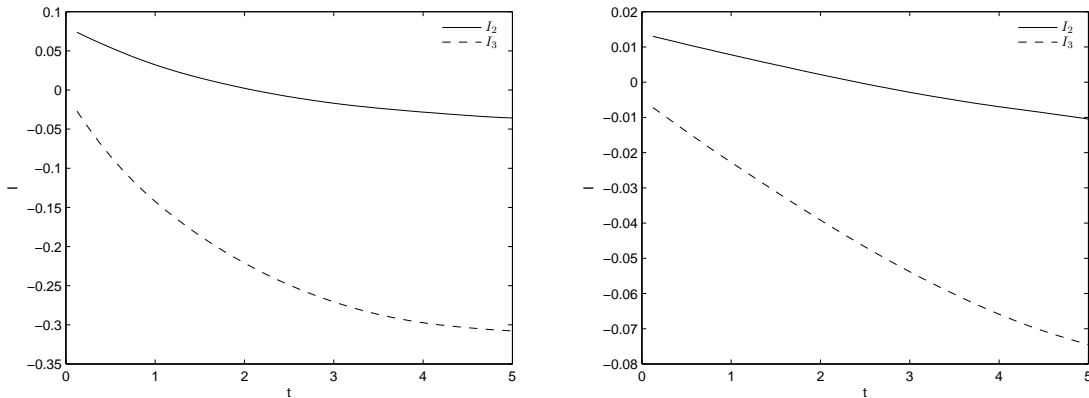


FIGURE 11. Variation of  $I_2, I_3$  with hydrodynamical damping, where  $\beta = 1$ ,  $\gamma = 2$ ,  $c = 1.1$ . Left:  $\nu = 0.1$ , right:  $\nu = 0.01$ .

#### 4. STOCHASTIC DAMPED WAVE EQUATION

In this section, we present some numerical results on behavior of different solitary waves in the presence of stochastic external force and damping effects. We will perform Monte Carlo simulations to obtain some significant statistical information. It is well known that a Monte Carlo simulation uses repeated sampling to determine the properties of specific phenomenon. In the framework of Monte Carlo simulations, we need specify a domain of possible inputs firstly, then generate realizations of inputs randomly from a prescribed probability distribution over the domain. For

each realization the data are fixed and a deterministic computation on the inputs is performed. Upon solving the deterministic equations with one realization, we can collect an ensemble of solutions. From these ensembles, the results can be aggregated and the influence of stochastic force on the propagation of solitary waves will be studied and the mean solitary wave height will be measured.

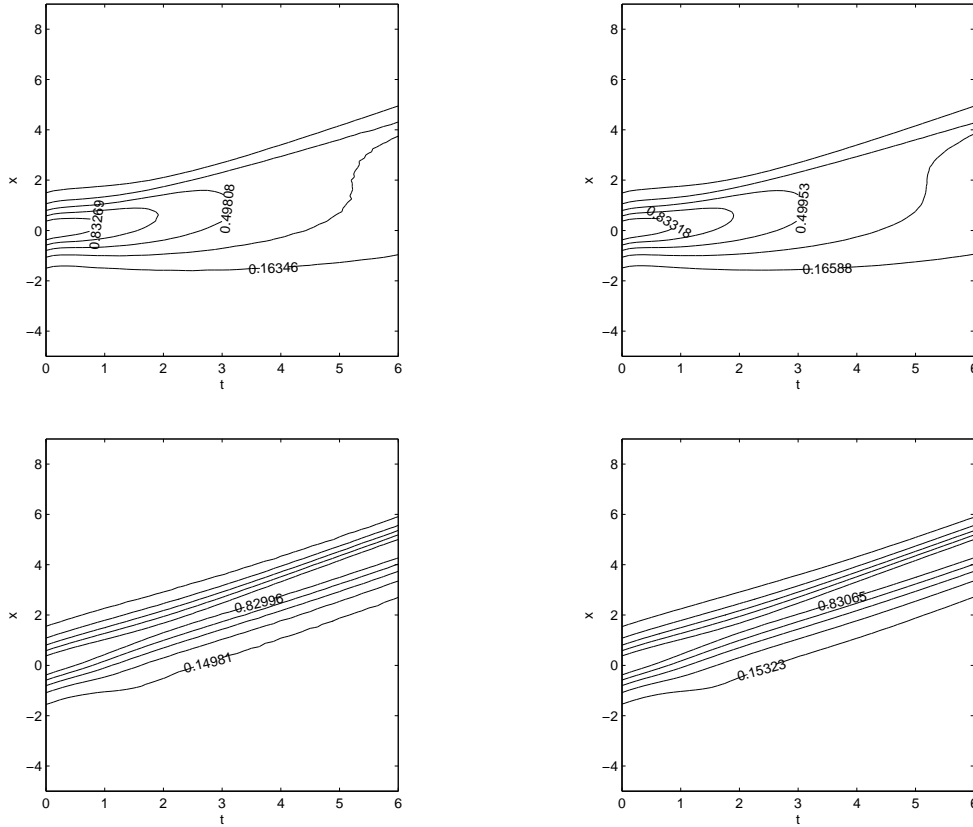


FIGURE 12. Contour plots of  $\langle u \rangle$  for soliton with Stokes damping and stochastic force, top left:  $\rho = 5$ ,  $\eta = 0.008$ , top right:  $\rho = 5$ ,  $\eta = 0.002$ , bottom left:  $\rho = 0.5$ ,  $\eta = 0.008$ , bottom right:  $\rho = 0.5$ ,  $\eta = 0.002$ .

**4.1. THE STOKES DAMPING AND NOISE.** (1) We first study the evolution of a single soliton in the presence of Stokes damping and noise. Such being the case, we set  $\alpha = \beta^2$ ,  $\beta > 0$ ,  $S(x, t) = \rho \partial_t u$  and  $f(u, x, t) = \gamma u^3$  in Equation (1.1). Initial condition (2.15) and Dirichlet boundary condition will be used and the simulation is took on  $(x, t) \in [-5, 9] \times (0, 6]$ . Our discrete scheme developed in section two with  $h = 2\Delta t$  is adopted. We first take  $\rho = 5$ ,  $\eta = 0.008$  and consider the behavior of single soliton under strong Stokes damping and noise with high level. The contour curves of the soliton of the 300 runs by MCS is presented in Figure 12 (top left). As can be seen, the soliton distorts significantly both on amplitude and width.

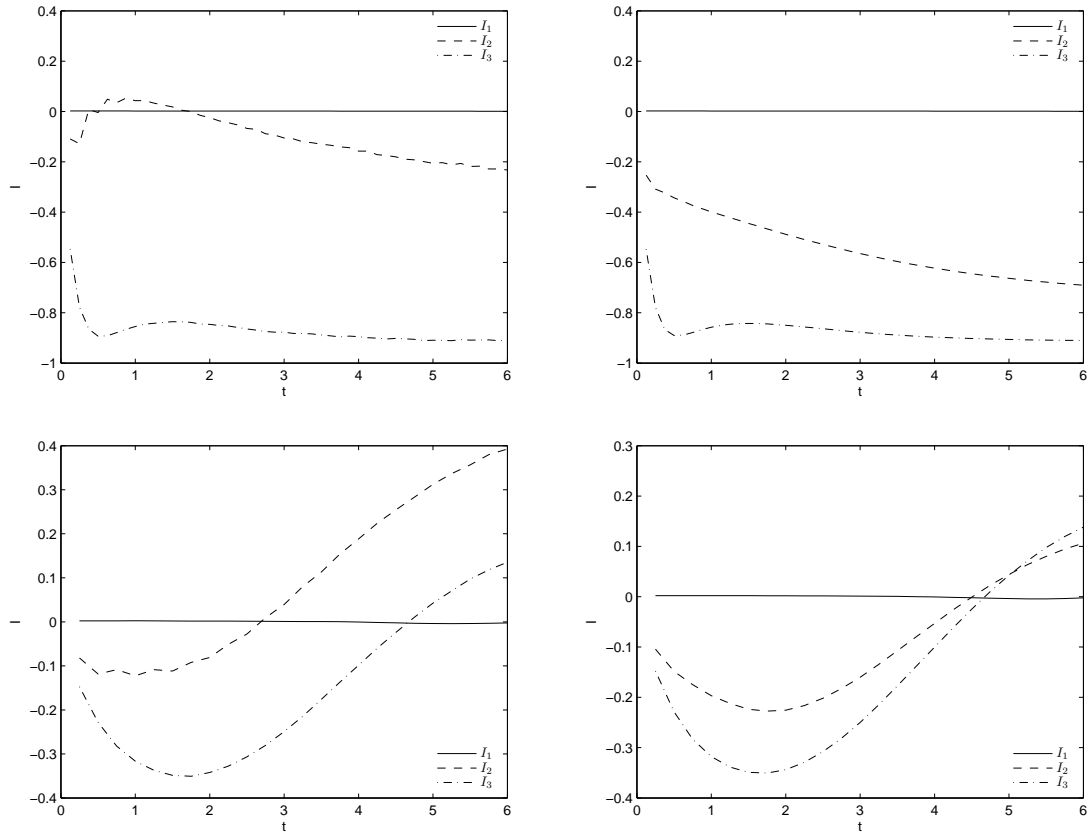


FIGURE 13. MCS results of  $I_1, I_2, I_3$  for soliton with Stokes damping and stochastic force, top left:  $\rho = 5, \eta = 0.008$ , top right:  $\rho = 5, \eta = 0.002$ , bottom left:  $\rho = 0.5, \eta = 0.008$ , bottom right:  $\rho = 0.5, \eta = 0.002$ .

In order to further reveal the influence of the stochastic force on the propagation of soliton, we have altered the amplitude of the stochastic force to  $\eta = 0.002$ . The other conditions are the same as the thereinbefore. In Figure 12 (top right), the results of the contour curves of the average of 300 runs is displayed. Again, the distortion of the soliton is observed, both on soliton height and wave width. By compare to the top left plot of Figure 12 which represent the  $\eta = 0.008$  case, we can find that the solitons behavior in a similar way. To say it in another way, there is no obvious difference between the two cases graphically, which indicate that the distortion of soliton is mainly caused by the Stokes damping effect. We have conduct simulations for the cases  $\rho = 0.5, \eta = 0.008$  and  $\rho = 0.5, \eta = 0.002$  by keeping other conditions and parameters invariant. The contour plots of the case with weak Stokes damping and two levels of noise are presented in Figure 12 (bottom). From the bottom plots of Figure 12 we can find out that the soliton is influenced by the Stokes damping and stochastic effects, while the soliton is not totally destroyed but keeping evolve with time. By comparing the bottom left plot and bottom right plot, no obvious difference

is observed graphically, which reveals the truth that the transformation of the soliton is mainly contributed to the Stokes effect.

The variation of  $\langle I_1 \rangle$ ,  $\langle I_2 \rangle$  and  $\langle I_3 \rangle$  with 300 runs are shown in Figure 13 (top left for  $\rho = 5$ ,  $\eta = 0.008$ , top right for  $\rho = 5$ ,  $\eta = 0.002$  and bottom left for  $\rho = 0.5$ ,  $\eta = 0.008$ , bottom right for  $\rho = 0.5$ ,  $\eta = 0.002$ ). It is very irregular of the individual trajectory curve, however, the curves derived from MCS have get rid of these oscillations to some extent. From Figure 13 we can get some conclusions as follows. (i) It seems that the quantity  $I_1$  keeps invariant in each case. From another point of view, it indicates that the quantity  $MA$  is conserved in the presence of Stokes damping and stochastic force in our simulation. Recall the results in Figure 5, we can deduced that the Stokes damping and stochastic force do not vary the value of  $MA$ . (ii) In view of the two plots on top which corresponds to  $\rho = 5$ , we can see that  $I_3$  evolves almost in a same way. In retrospect the result in Figure 5 (left), the noise has little influence on  $I_3$  is a reasonable explanation. Similar conclusion can be deduced for  $I_3$  on the bottom plots. (iii) Concerning  $I_2$  in top two plots,  $I_2$  in the top left case evolves in a different way by comparing to the top right case. More precisely,  $I_2$  in the top left experience a first climb then decline process while it declines monotonously in the top right case. Review the result in Figure 5 (left), it seems that the noise influenced  $I_2$  to some extent.

(2) We now investigate the influence of the Stokes damping and stochastic force on the propagation of kink wave. The parameters and initial boundary conditions are by the same settings as in the Stokes damping case. To begin with, we first take  $\eta = 0.008$  and consider the behavior of kink solution under strong noise effect with different damping strength. The level curves of the kink solution of the 300 runs by MCS are presented in Figure 14 (top left for  $\rho = 5$ , bottom left for  $\rho = 0.5$ ). The kink distorts phenomena are observed in both plots. In order to further study the influence of the stochastic force on the propagation of kink solution, we have varied the amplitude of the noise to  $\eta = 0.002$ . The other conditions are keep invariant. In Figure 14, the results of the level curves of the average of 300 runs are displayed (top right for  $\rho = 5$ , bottom right for  $\rho = 0.5$ ). Again, the distortion of the kink wave is observed. From another point of view, the top two plots correspond to Stokes damping with strong strength. By compare to the top left plot of Figure 14 which represent the  $\eta = 0.008$  case, we can find that the kink behavior on the top right plot is very similarly. It follows that there is no obvious difference between the two cases graphically, which indicate that the distortion of kink is mainly caused by the Stokes effect. By the same token, the bottom plots of Figure 14 indicate that the kink wave is influenced by the Stokes damping and stochastic effects, while the kink is not totally destroyed and keeping evolve with respect to time. By comparing the bottom left plot and the bottom right plot, no obvious difference is observed graphically, which

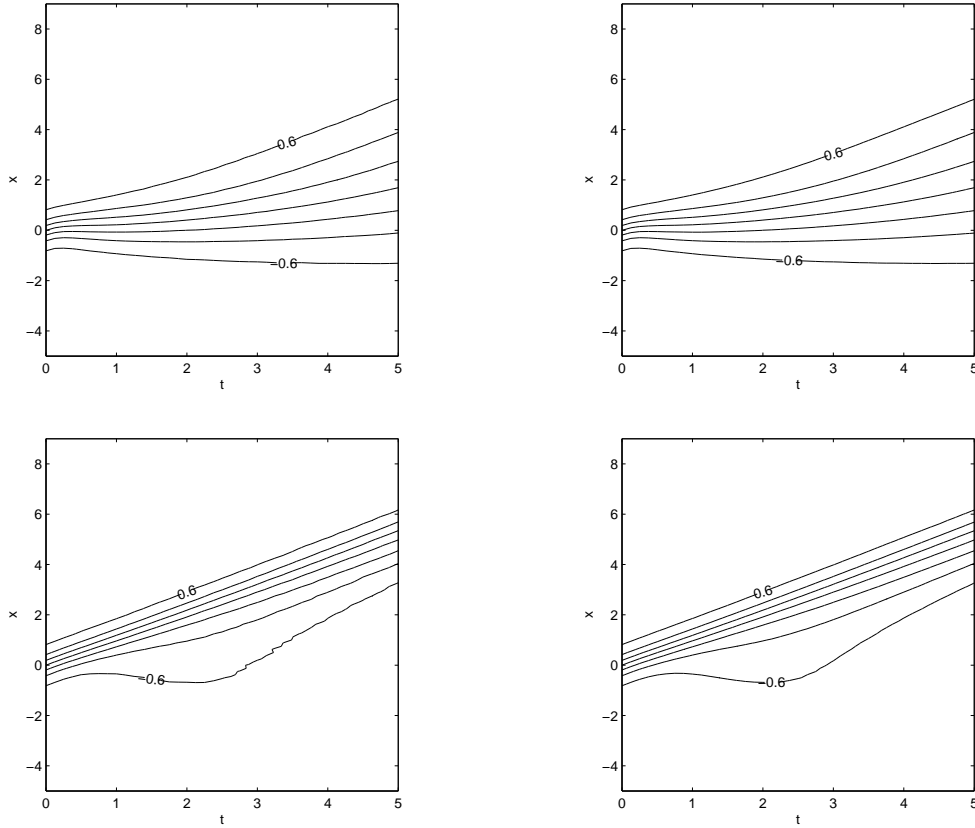


FIGURE 14. Contour plots of  $\langle u \rangle$  for kink solution with Stokes damping and stochastic force, top left:  $\rho = 5, \eta = 0.008$ , top right:  $\rho = 5, \eta = 0.002$ , bottom left:  $\rho = 0.5, \eta = 0.008$ , bottom right:  $\rho = 0.5, \eta = 0.002, \beta = 1, \gamma = 2, c = 1.1$ .

reveals the truth that the variation of the kink wave is mainly contributed to the Stokes damping. The variation of  $\langle I_2 \rangle$  and  $\langle I_3 \rangle$  with 300 runs are shown in Figure 15 (top left for  $\rho = 5, \eta = 0.008$ , top right for  $\rho = 5, \eta = 0.002$  and bottom left for  $\rho = 0.5, \eta = 0.008$ , bottom right for  $\rho = 0.5, \eta = 0.002$ ). From Figure 15 we can get some conclusions as follows. (i) Under the circumstance of strong Stokes damping, it seems that the quantity  $I_2$  and  $I_3$  are mainly influenced by Stokes effect, which is confirmed by the fact that the two top plots behavior no obvious difference. (ii) Concerning  $I_2$  in the two plots on bottom which corresponds to  $\rho = 0.5$ ,  $I_2$  in the bottom left case evolves in a different way by comparing to the bottom right case. More precisely,  $I_2$  in the bottom left experience a climb process. Review the result in Figure 7 (right), it seems that the noise influenced  $I_2$  to some extent in this situation.

**4.2. THE HYDRODYNAMICAL DAMPING AND NOISE. (1)** Here we check the effect of stochastic force and hydrodynamical damping on the propagation of single soliton. The initial boundary conditions and the parameters are the same

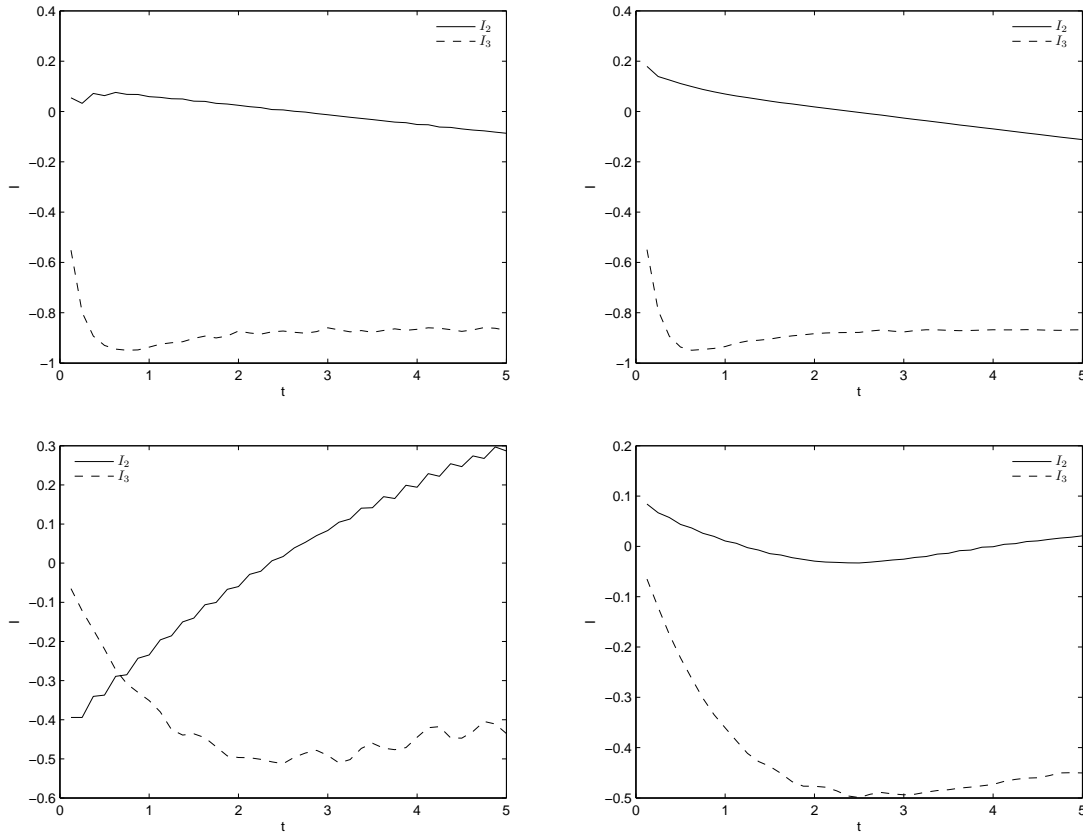


FIGURE 15. MCS results of  $I_2, I_3$  with Stokes damping and stochastic force, top left:  $\rho = 5, \eta = 0.008$ , top right:  $\rho = 5, \eta = 0.002$ , bottom left:  $\rho = 0.5, \eta = 0.008$ , bottom right:  $\rho = 0.5, \eta = 0.002$ , kink with  $\beta = 1, \gamma = 2, c = 1.1$ .

as that in hydrodynamical effect case. We begin with  $\eta = 0.008$  and investigate the behavior of single soliton under hydrodynamical damping and stochastic force. The contour plots of soliton computed by MCS with 300 runs are shown in Figure 16 (top left for  $\nu = 0.1$ , bottom left for  $\nu = 0.01$ ). For the sake of further investigate the influence of the noise on the propagation of soliton, we have varied the strength of the stochastic force to  $\eta = 0.002$ . The remainder conditions are the same as above. In Figure 16 (bottom right for  $\nu = 0.1$ , bottom right for  $\nu = 0.01$ ), the evolution of soliton under this setting is displayed in the form of level curves. The main line present the propagation of the soliton. The numbers on the level curves denote the mean height of soliton in each plot. Based on the observation that the soliton continues to evolve at a velocity which is close to the initial one. The change of the soliton shape is observed. By comparison of the plots in Figure 16 and in Figure 8, we can find out that the noise contaminate the soliton to some extent, while it will not totally destroy the soliton propagation.

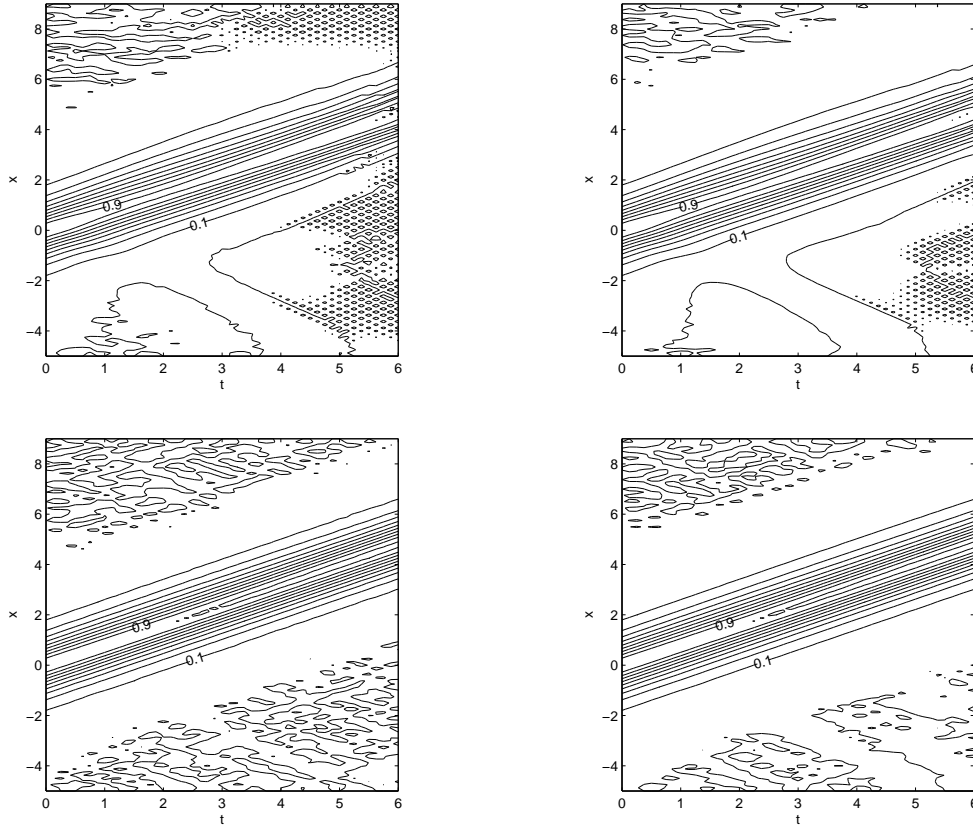


FIGURE 16. Contour plot of soliton with hydrodynamical damping and noise where  $\beta = 1$ ,  $\gamma = 2$ ,  $c = 0.8$ . Top left:  $\nu = 0.1$ ,  $\eta = 0.008$ , top right:  $\nu = 0.1$ ,  $\eta = 0.002$ , bottom left:  $\nu = 0.01$ ,  $\eta = 0.008$ , bottom right:  $\nu = 0.01$ ,  $\eta = 0.002$

Figure 17 shows the evolution of averaged  $I_1$ ,  $I_2$ ,  $I_3$  estimated by 300 trajectories which are integrated on the time interval  $[0, 6]$ , top left for the case  $\nu = 0.1$ ,  $\eta = 0.008$ , top right for the case  $\nu = 0.1$ ,  $\eta = 0.002$ , bottom left for the case  $\nu = 0.01$ ,  $\eta = 0.008$  and bottom right corresponds to  $\nu = 0.01$ ,  $\eta = 0.002$ . In view of these plots we can conclude several facts as follows. (i) In all four cases the quantity  $I_1$  is almost keeps invariant. By recall the results revealed in Figure 9, it is rational to conclude that  $I_1$  is immune from hydrodynamical damping and stochastic effect in our simulation. (ii) According to the top two plots, it is seems that the hydrodynamical damping with strong strength dominating the influences on  $I_2$  and  $I_3$ . Furthermore, in retrospect the result in Figure 9, the noise effect on  $I_2$  and  $I_3$  is negligible when compared to hydrodynamical damping with strong strength. (iii) The bottom two plots indicate that the noise effect dominate the influence on  $I_2$  and  $I_3$  when there exist hydrodynamical damping with weak strength.

(2) We are now in a position to investigate the influence of the hydrodynamical damping and stochastic force on the evolution of kink wave. The parameters and

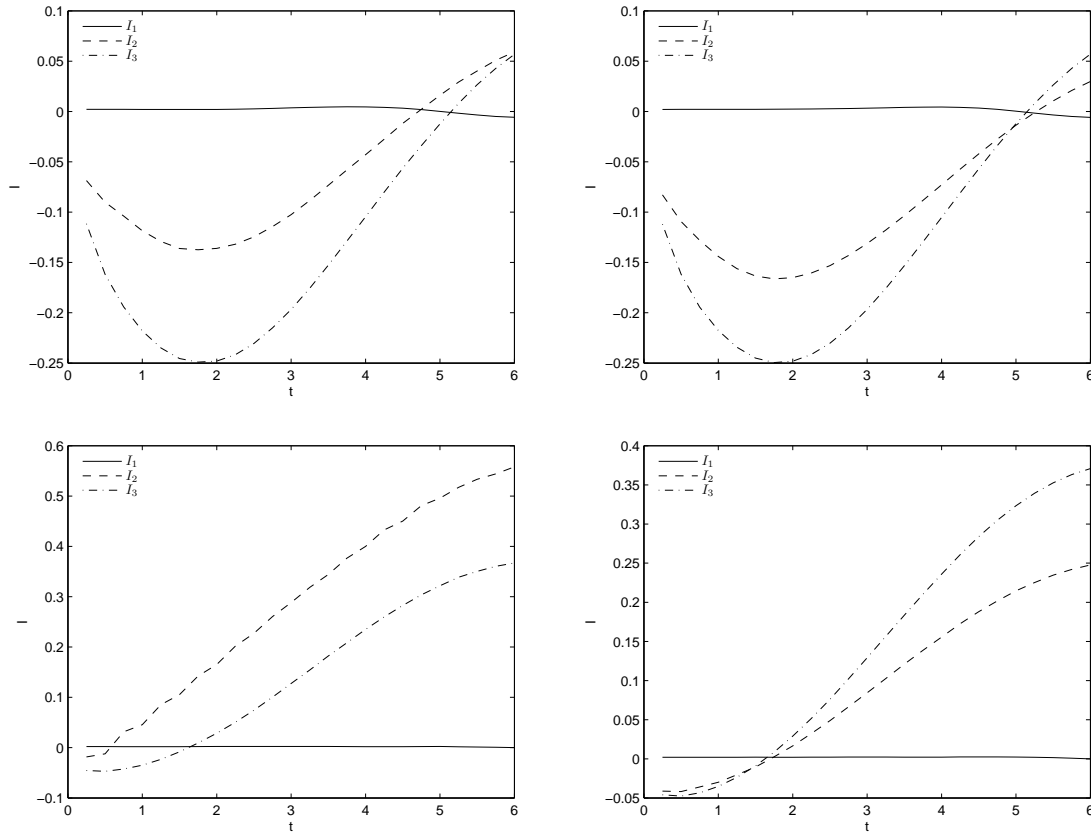


FIGURE 17. MCS results of  $I_1, I_2, I_3$ , where  $\beta = 1, \gamma = 2, c = 0.8$ .  
 Top left:  $\nu = 0.1, \eta = 0.008$ , top right:  $\nu = 0.1, \eta = 0.002$ , bottom left:  
 $\nu = 0.01, \eta = 0.008$ , bottom right:  $\nu = 0.01, \eta = 0.002$

initial boundary conditions are the same as the hydrodynamical damping case. Figure 18 reports different level curves derived by MCS with 300 trajectories on the interval of time  $[0, 5]$  for  $\eta = 0.008$  and  $\eta = 0.002$  with different damping strength. The number on the level curves represent the mean kink wave height in the figure. Graphically, there is no obvious observable difference between the two situations on the top plots, showing that the effect of the presence of stochastic force is not important for the kink wave propagation under this case. Similar conclusion can be derived for the bottom plots. Figure 19 displays the variation of  $\langle I_2 \rangle, \langle I_3 \rangle$  derived from MCS with 300 runs (top left for  $\rho = 5, \eta = 0.008$ , top right for  $\rho = 5, \eta = 0.002$  and bottom left for  $\rho = 0.5, \eta = 0.008$ , bottom right for  $\rho = 0.5, \eta = 0.002$ ). Some conclusions can be derived from Figure 19 as follows. (i) In the situation of strong hydrodynamical damping, it seems that the quantity  $I_2$  and  $I_3$  are mainly influenced by damping effect, which is confirmed by the fact that it is hard to distinguish between the two top plots. (ii) Concerning  $I_2$  in the two plots on bottom which corresponds to  $\rho = 0.5$ ,  $I_2$  in the bottom left plot behavior in a different way by comparing to the bottom right plot. More precisely,  $I_2$  in the bottom left experience a climb process. Review

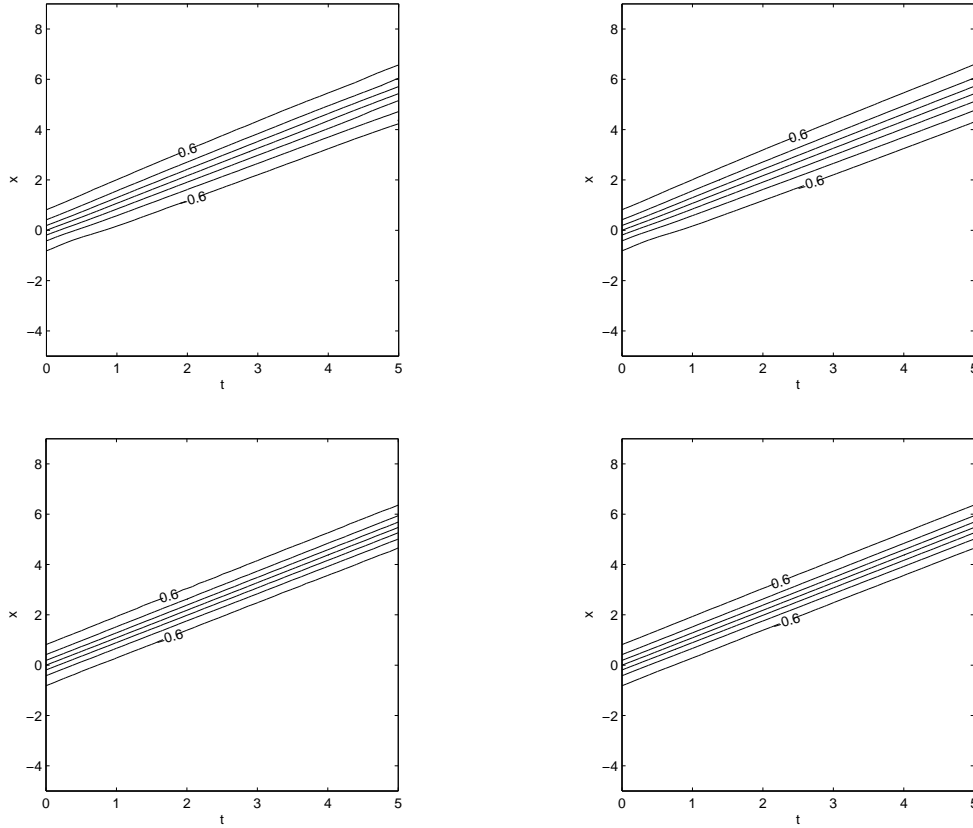


FIGURE 18. Contour plot of kink with hydrodynamical damping and noise. Top left:  $\nu = 0.1$ ,  $\eta = 0.008$ , top right:  $\nu = 0.1$ ,  $\eta = 0.002$ , bottom left:  $\nu = 0.01$ ,  $\eta = 0.008$ , bottom right:  $\nu = 0.01$ ,  $\eta = 0.002$ ,  $\beta = 1$ ,  $\gamma = 2$ ,  $c = 1.1$ .

the result in Figure 11 (right), it seems that the stochastic with high level influenced  $I_2$  to some extent in this situation.

## 5. CONCLUSION

In this paper, we have numerically studied a nonlinear wave equation in the presence of damping and stochastic force. A quadratic finite volume element scheme is proposed for the considered problem. Numerical results demonstrate that the scheme is robust and efficient for solving the nonlinear wave equation. The damping effect with strong strength would destroy the propagation of solitary wave and kink wave. Stokes damping has a stronger influence than the hydrodynamical damping on the evolution of soliton. In addition, there is a quantity namely  $MA$  conserved both in the presence of Stokes damping and noise. Energy and momentum will no longer keep invariant under damping and stochastic force. Furthermore, noise will dominate the influence on energy and momentum in the case of weak damping. On the other hand, stochastic effect is negligible in the presence of strong damping. Concerning

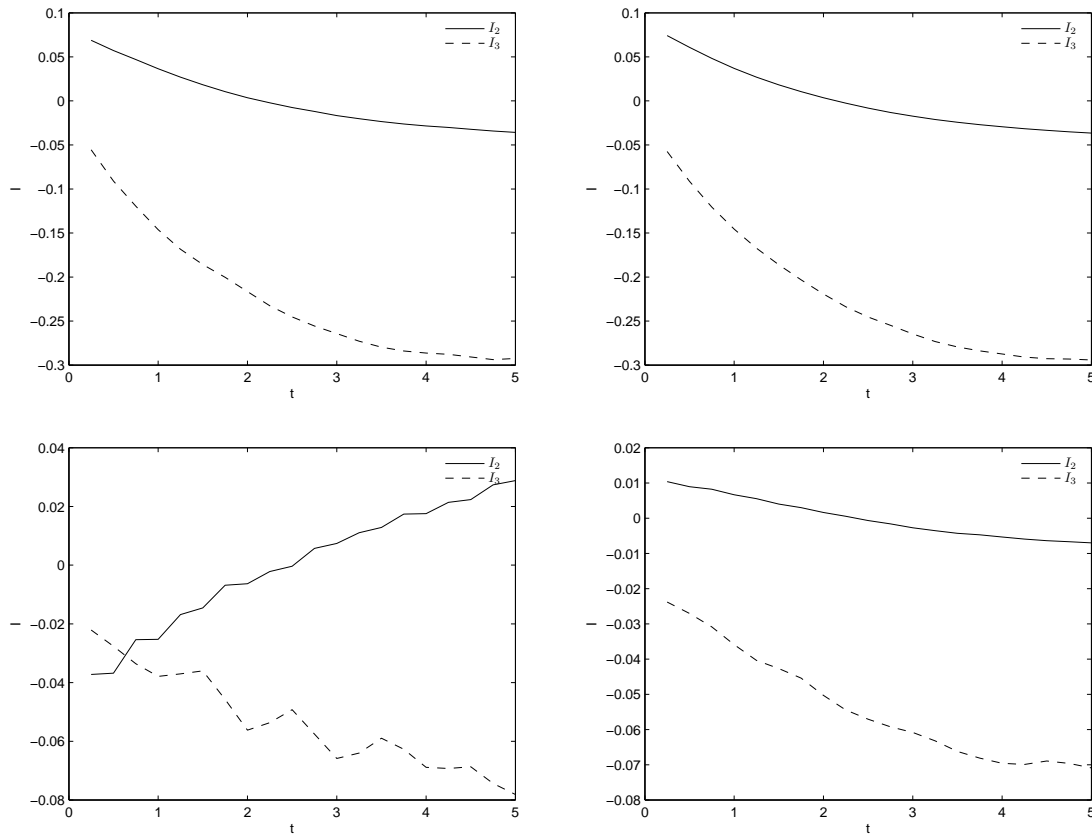


FIGURE 19. MCS results of  $I_2, I_3$ , where  $\beta = 1, \gamma = 2, c = 1.1$ . Top left:  $\nu = 0.1, \eta = 0.008$ , top right:  $\nu = 0.1, \eta = 0.002$ , bottom left:  $\nu = 0.01, \eta = 0.008$ , bottom right:  $\nu = 0.01, \eta = 0.002$ .

individual trajectory, the existence of the noise will contaminate the evolution of soliton. Nevertheless, MCS analysis of the problem indicate that the stochastic force affect little on the propagation of the soliton in average.

### ACKNOWLEDGMENTS

This work is supported by the National Natural Science Foundation of China (No. 11447017,11471166), the Fundamental Research Funds for the central Universities (No. KYZ201565), Zhejiang Provincial Natural Science Foundation of China (No. Y14A010016, LY13A010008, LY13F020020) and public projects of Lishui Science and Technology Bureau(No. 2013JYZB18).

### REFERENCES

- [1] S. Goldstein. On diffusion by discontinuous movements, and on the telegraph equation. *The Quarterly Journal of Mechanics and Applied Mathematics*, 4(2):129–156, 1951.
- [2] J. Biazar and M. Eslami. Analytic solution for telegraph equation by differential transform method. *Physics Letters A*, 374(29):2904–2906, 2010.

- [3] R.K. Mohanty. New unconditionally stable difference schemes for the solution of multi-dimensional telegraphic equations. *International Journal of Computer Mathematics*, 86(12):2061–2071, 2009.
- [4] M. Dehghan and A. Shokri. A numerical method for solving the hyperbolic telegraph equation. *Numerical Methods for Partial Differential Equations*, 24(4):1080–1093, 2008.
- [5] R.K. Mohanty, M.K. Jain, and U. Arora. An unconditionally stable adi method for the linear hyperbolic equation in three space dimensions. *International Journal of Computer Mathematics*, 79(1):133–142, 2002.
- [6] J. Shatah. Normal forms and quadratic nonlinear klein-gordon equations. *Communications on Pure and Applied Mathematics*, 38(5):685–696, 1985.
- [7] W. Strauss and L. Vazquez. Numerical solution of a nonlinear klein-gordon equation. *Journal of Computational Physics*, 28(2):271–278, 1978.
- [8] C.S. Jia, T. Chen, and S. He. Bound state solutions of the klein-gordon equation with the improved expression of the manning-rosen potential energy model. *Physics Letters A*, 377(9):682–686, 2013.
- [9] K. Nakanishi and W. Schlag. Global dynamics above the ground state energy for the focusing nonlinear klein-gordon equation. *Journal of Differential Equations*, 250(5):2299–2333, 2011.
- [10] M.J. Ablowitz, D.J. Kaup, A.C. Newell, and H. Segur. Nonlinear-evolution equations of physical significance. *Physical Review Letters*, 31(2):125–127, 1973.
- [11] G. Leibbrandt. New exact solutions of the classical sine-gordon equation in 2+1 and 3+1 dimensions. *Physical Review Letters*, 41(7), 1978.
- [12] A.M. Wazwaz. Compactons, solitons and periodic solutions for some forms of nonlinear klein-gordon equations. *Chaos, Solitons & Fractals*, 28(4):1005–1013, 2006.
- [13] A.G. Bratsos. The solution of the two-dimensional sine-gordon equation using the method of lines. *Journal of Computational and Applied Mathematics*, 206(1):251–277, 2007.
- [14] M. Dehghan, A. Mohebbi, and Z. Asgari. Fourth-order compact solution of the nonlinear klein-gordon equation. *Numerical Algorithms*, 52(4):523–540, 2009.
- [15] K. Djidjeli, W.G. Price, and E.H. Twizell. Numerical solutions of a damped sine-gordon equation in two space variables. *Journal of Engineering Mathematics*, 29(4):347–369, 1995.
- [16] C.X. Zheng. Numerical solution to the sine-gordon equation defined on the whole real axis. *SIAM Journal on Scientific Computing*, 29(6):2494–2506, 2007.
- [17] R.H. Li, Z.Y. Chen, and W. Wu. *Generalized difference methods for differential equations: numerical analysis of finite volume methods*, volume 226. CRC Press, 2000.
- [18] J. Li and Z.X. Chen. A new stabilized finite volume method for the stationary stokes equations. *Advances in Computational Mathematics*, 30(2):141–152, 2009.
- [19] E. Platen. *An introduction to numerical methods for stochastic differential equations*. Cambridge University Press, 1999.
- [20] J.S. Liu. *Monte Carlo strategies in scientific computing*. Springer, 2008.